HAL open science

Hycell: a new hybid model of the rain horizontal distribution for propagation studies. Part 1: Modelling of the rain cell.

L. Féral, Henri Sauvageot, L. Castanet, J. Lemorton

▶ **To cite this version:**

L. Féral, Henri Sauvageot, L. Castanet, J. Lemorton. Hycell: a new hybid model of the rain horizontal distribution for propagation studies. Part 1: Modelling of the rain cell.. Radio Science, 2003, 38, pp.1056. 10.1029/2002RS002802 . hal-00137818

HAL Id: hal-00137818

https://hal.science/hal-00137818v1

Submitted on 24 Jan 2022

HAL is a multi-disciplinary open access archive for the deposit and dissemination of scientific research documents, whether they are published or not. The documents may come from teaching and research institutions in France or abroad, or from public or private research centers.

L'archive ouverte pluridisciplinaire **HAL**, est destinée au dépôt et à la diffusion de documents scientifiques de niveau recherche, publiés ou non, émanant des établissements d'enseignement et de recherche français ou étrangers, des laboratoires publics ou privés.

Distributed under a Creative Commons Attribution 4.0 International License

HYCELL—A new hybrid model of the rain horizontal distribution for propagation studies: 1. Modeling of the rain cell

Laurent Féral

Département Electromagnétisme et Radar, Office National d'Etudes et de Recherches Aérospatiales, Toulouse, France

Henri Sauvageot

Observatoire Midi-Pyrénées, Laboratoire d'Aérologie, Université Paul Sabatier, Toulouse, France

Laurent Castanet and Joël Lemorton

Département Electromagnétisme et Radar, Office National d'Etudes et de Recherches Aérospatiales, Toulouse, France

Received 24 October 2002; revised 24 February 2003; accepted 28 March 2003; published 13 June 2003.

[1] From radar observations of rain fields at midlatitudes, a new physical model of rain cells is proposed. It strives to describe optimally the rain rate horizontal distribution within rain cells down to 1 mm h^{-1}. The approach is similar to that of the well-known EXCELL model. The mathematical definition of the model lies in the combination of a gaussian function and an exponential one, the cells having an elliptic horizontal cross section. Due to its hybrid structure, the new model has been named HYCELL. From a conceptual point of view, the gaussian component describes the convective-like high rain rate core of the cell, while the exponential component accounts for the surrounding stratiform-like low rain rate spreading down to 1 mm h^{-1}. The modeling of a rain cell with HYCELL then requires the determination of seven parameters. The latter is obtained, cell by cell, by solving a set of five fit-forcing equations completed by two continuity equations. The fit-forcing equations involve radar parameters of integral nature which refer not only to the rain cell geometry (area, ellipticity) but also to the rain rate R distribution inside the cell (mean and root mean square values of R and gradient of R). Their analytical expressions are derived from the model definition, while their values are forced to be those derived from radar measurements. Using this method, thousands of rain cells identified from radar observations in the regions of Bordeaux (southwestern France) and Karlsruhe (southwestern Germany) have been modeled. Though both sites are at midlatitude, the climatic contexts differ: oceanic for Bordeaux and continental for Karlsruhe. Results of rain rate horizontal distribution modeling within cells using HYCELL and EXCELL are compared. It is then suggested that the HYCELL model is a new tool which deserves to be considered by system designers to compute propagation parameters. *INDEX TERMS:* 3354 Meteorology and Atmospheric Dynamics: Precipitation (1854); 3210 Mathematical Geophysics: Modeling; 3360 Meteorology and Atmospheric Dynamics: Remote sensing; 6964 Radio Science: Radio wave propagation; *KEYWORDS:* propagation in rain, radar meteorology, rain modeling

Citation: Féral, L., H. Sauvageot, L. Castanet, and J. Lemorton, HYCELL—A new hybrid model of the rain horizontal distribution for propagation studies: 1. Modeling of the rain cell, *Radio Sci.*, *38*(3), 1056, doi:10.1029/2002RS002802, 2003.

1. Introduction

[2] The telecommunication evolution for fixed satellites depends on the users' increasing need for accessing to multimedia services. It results in the necessity to

Copyright 2003 by the American Geophysical Union.
0048-6604/03/2002RS002802

convey higher and higher data rates and, due to the congestion of conventional frequency bands (L, S, C and Ku-bands), compels to use of frequencies higher than 20 GHz. This frequency shift raises problems related to the influence of the atmosphere, and notably of the precipitation, on the electromagnetic propagation [*Castanet et al.*, 2001; *Lemorton et al.*, 2001].

[3] Now, in order to be attractive for users, operators will have to offer an availability comparable to the one usually reached by systems operating at lower frequency bands, such as Ku-band, which can be done through the implementation of Fade Mitigation Techniques [*Castanet et al.*, 2002a, 2002b]. That is the reason it is useful for system designers to dispose of a thorough knowledge of the rain field horizontal structure, so as to evaluate system parameters such as attenuation, depolarization, and scattering interference, to finally improve the service availability by optimizing the satellite resource management.

[4] On the one hand, the description of the rain field horizontal structure is difficult due to its high space-time variability, explaining the statistical nature of most of the studies on the subject. Thus, for example, many authors have developed empirical or statistical models of rain cell size distribution based on radar measurements [*Konrad*, 1978; *Goldhirsh and Musiani*, 1986; *Crane*, 1996; *Mesnard and Sauvageot*, 2003].

[5] On the other hand, from meteorological studies, more and more is known about the physical processes which govern the structure of rain cells. Obviously, the physical modeling of the latter would be very useful for system designers having to predict, in a realistic way and from a small number of parameters, single site attenuation and joint statistics for a pair of paths required in the design of space diversity systems and rain interference coupling between two intersecting paths [e.g., *Rogers*, 1972; *Lane and Stutzman*, 1980; *Crane*, 1982; *Crane and Shieh*, 1989]. Indeed, considering modeled cells - that is cells described by a small number of parameters - would allow to reduce considerably the computing time and storage problems and also to multiply the system simulations to optimally define the system parameters.

[6] In this context, *Capsoni et al.* [1987a, 1987b] proposed to model the horizontal structure of rain cells by the EXCELL model. According EXCELL, the rain cells are of elliptic shape and the rain rate R within the cells decays exponentially around a single maximum. In its primary formulation, the EXCELL model was defined and validated from radar observations at midlatitude (Milan, Italy) of 6215 rain cells identified by thresholding the rain fields at R = 5 mm h^{-1}, so that the validity domain of EXCELL is $R \geq 5$ mm h^{-1}. When it was devised, the EXCELL model met the requirements of system designers to predict propagation parameters in telecommunication applications at X and Ku-bands, since the attenuation by rain rates lower than 5 mm h^{-1} is not very high for these frequency bands. That is the reason why EXCELL was especially dedicated to the description of the rain rate horizontal distribution within the cells for $R \geq 5$ mm h^{-1}.

[7] In other respects, when considering radar observations of rain fields, it becomes clear that important information lays in areas over which the rain rate is weaker than 5 mm h^{-1}. Indeed, the probability of occurrence of a rain rate higher than 5 mm h^{-1} is smaller than about 10% at midlatitude [e.g., *Sauvageot*, 1994]. In fact, neglecting these small rain rates leads to ignore not only the rain cells stratiform spreading but also the high percentage of cells with a peak rain rate lower than 5 mm h^{-1}. Now, these rainy areas, due to their spatial extent, play an important part in the attenuation endured by radio links, especially at the high frequencies envisaged for the future satellite telecommunication systems. Therefore, *Paraboni et al.* [1998, 2002] proposed an extended version of EXCELL, applicable down to a zero rain rate for use in low margin systems. The new "lowered" EXCELL model is not fully determinist insofar as it involves a rain cell lowering parameter which is statistical in nature, since deduced from the local cumulative distribution function of the rainfall intensity.

[8] In the present paper, a new physical model of rain cells is proposed, using an approach similar to that of the EXCELL model. The new model lies on the combination of a gaussian function and an exponential one. Its physical foundations are explained in section 2. As for the EXCELL model, it is defined, cell by cell, by forcing appropriate cell descriptors of integral nature to be the same as those obtained from the radar observations. The modeling methodology is fully described in section 3. From radar observations of rain fields in two regions both at midlatitude but with different climates, more than 900,000 rain cells are modeled. Various comparative results are given in section 4, showing the ability of the new model to describe the rain rate horizontal distribution within the cells, whatever their climatological belonging.

2. Rain Cell Definition

[9] In the studies of rain fields from meteorological radar observations, authors refer to the terms "rain cell" or "rain area" to describe the patchy structure of the rain. The term "Cell" seems to be preferred when there is an explicit or implicit reference to the associate dynamic structure as the cause of rain. When discussing the structure of rain field without considering the peak number inside the rain entities as a criterion of classification, it seems more correct to use the term "rain area." In the past, in the literature about the rain field structure in relation with the radioelectric propagation, the above distinction was not considered and the term "rain cell" was mainly used [*Misme and Waldteufel*, 1980; *Crane*,

1982, 1996; *Crane and Shieh*, 1989; *Capsoni et al.*, 1987a, 1987b]. In the present work, focused on the propagation problem, this convention is used, firstly not to confuse the reader and, secondly, because we consider mainly rain entities of small area and because, as will be recalled below, most small rain areas have a single maximum and thus deserve to be termed "cell."

[10] In the literature, rain cells have been defined mainly in two ways. First, as the area interior to a closed contour, down a local maximum (or peak) of the reflectivity by 3 to 10 dB and surrounding this local maximum [e.g., *Konrad*, 1978; *Crane*, 1996]. Secondly, when analyzing the structural characteristics of a rain field with respect to a rain rate threshold τ, the rain cell is defined as the area inside which the rain rate $R \geq \tau$ [e.g., *Drufuca*, 1977; *Goldhirsh and Musiani*, 1986]. The cell is continuous and, along the contour that bounds it, the rain rate is equal to the threshold value τ. This study considers the second definition since its aim is a rain cell modeling including the stratiform component.

[11] As part of a rain cell modeling, the choice of the physical model has to be carefully justified, for it has to account for the rain cell shape and for the rain rate horizontal distribution within the cell. From radar observations of rain field, many authors [*Dennis and Fernald*, 1963; *Miller et al.*, 1975; *Konrad*, 1978; *Goldhirsh and Musiani*, 1986; *Tenorio et al.*, 1995; *Sauvageot et al.*, 1999] have considered that rain cells can be approximated to a circular shape. The diameter of the circular cell of equivalent area is used as a characteristic measure of the rain cell size.

[12] *Pawlina and Binaghi* [1995] and *Féral et al.* [2000] questioned the validity of this approach and proposed to describe the rain cell shape by its equivalent ellipse, whose parameters are the major axis, the minor axis, and the orientation angle. Whatever the threshold, the results show that the rain cell orientation distribution is uniform while the distribution of the rain cell ellipticity, defined as the ratio of the minor to major axis, indicates that the majority of the small cells are twice longer than wide. Nevertheless, it can be observed that the ellipticity of the rain cells tends to 1 as their size increases. Therefore, whatever the threshold, rain cell horizontal cross sections can be reasonably approximated by ellipses.

[13] Concerning the rain rate horizontal distribution within the cells, many authors have divided the rain cell population into two groups: the stratiform cells, characterized by a slow decay of the rain rate from its maximum (which is usually chosen less than 10 mm h^{-1}), and the convective cells, generating an area of heavy rain with intensities higher than 10 mm h^{-1}. Usually, convective cells are surrounded by a stratiform area where the rain rate is weaker. These basic considerations underline the difficulty to model the rain rate horizontal distribution within the cells by means of a single mathematical function. Indeed, if an exponential function, as defined by *Capsoni et al.* [1987b], accounts for the spatial extent of the stratiform component, it is not always adapted to the description of the rain rate horizontal distribution in the convective part of the cell. Moreover, isolated punctual maxima of the rain rate are not observed in nature. In fact, radar observations show that, at all latitudes, the rain rate horizontal distribution in the vicinity of the rain cell peak does not decay as abruptly as what an exponential function would describe but rather as what a gaussian one would. As typical examples, Figure 1 shows the vertical cross section of a convective storm cell, observed by an S-band radar in southwestern France on 10 August 1996, while Figure 2 displays the temporal evolution (hyetograph) of the rain rate measured at the ground with a rain gauge in the region of Niamey (Niger, Sahelian Africa) on 03 September 1988. The rain cell in Figure 2 is part of a squall line moving westward with a velocity v of about 60 km h^{-1} (the usual value in the sahelian area), in such a way that the time scale t can be converted into horizontal distance. These figures both underline the gaussian character of the rain rate distribution in the vicinity of the rain cell peak.

[14] Now, a gaussian function is not always able to account for the surrounding stratiform component, which suggests the modeling of the rain rate horizontal distribution within the cells by combining a gaussian function and an exponential one.

[15] However, the rain cell modeling by means of unimodal functions would lead to consider that the rain rate horizontal distribution within a cell is organized around a single peak. Are all the rain cells single-peaked? Of course they are not: it is well-known that rain cells, especially when they are identified by thresholding at values as weak as 1 mm h^{-1}, can enclose several subcells or secondary maxima. Figure 2 can be seen as a typical example. Nevertheless, from radar observations of rain fields in tropical and midlatitudes areas, *Mesnard and Sauvageot* [2003] show that 95% of the rain cells having an equivalent diameter smaller than 5 km - which represents the majority of the cells - are single-peaked. Moreover, they show that, in average, the relative frequency of the rain cell as a function of their peak number p, that is $N_A(p)$, is well-approximated by the power distribution:

$$N_A(\mathrm{p}) = 0.71\ \mathrm{p}^{-2.77}. \tag{1}$$

According to (1), both for tropical and midlatitude areas, 71% of the rain cells are single-peaked. For the remaining 29%, a reasonable assumption is to consider that, from a statistical point of view, among the population of multipeaked cells, those inside which several convective areas of comparable intensity coexist

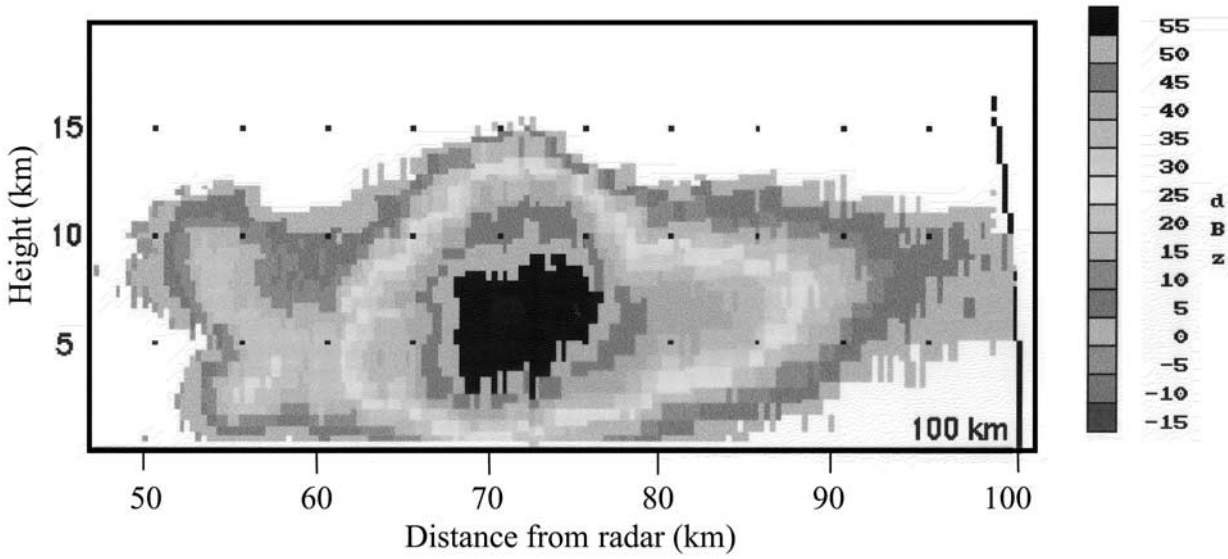

Figure 1. Vertical cross section (RHI) of a rain cell observed with an S-band radar in the region of Lannemezan (southwestern France) on 10 August 1996.

are rather infrequent, giving credibility to the rain cell modeling by unimodal mathematical functions.

[16] To sum up, from the above discussion, it can be concluded that (1) the rain cell shape can be approximated by an ellipse; (2) the rain rate horizontal distribution within the cells can be modeled by unimodal functions; (3) the present paper proposes to define a hybrid model, resulting from the combination of a gaussian component and an exponential one.

3. Modeling the Horizontal Structure of Rain Cells

3.1. EXCELL Model

[17] *Capsoni et al.* [1987b] proposed to describe the horizontal structure of rain cells by considering an exponential decay of the rain rate R around a single maximum of R, with an elliptic horizontal shape. This is the well-known EXCELL model according to which the analytical expression of the rain rate horizontal distribution within a cell is given in the horizontal plane (Oxy) by:

$$R(x, y) = R_E \exp\left[-\left(\frac{x^2}{a_E^2} + \frac{y^2}{b_E^2}\right)^{1/2}\right] \text{for} \quad R \geq R_2. \quad (2)$$

R_E is the peak rain rate, a_E and b_E are the distances along the axes (Ox) and (Oy) for which the rain rate decreases by a factor 1/e with respect to R_E (e.g., Figure 3b), respectively. Let R_2 be the minimum observed rain rate value. It defines the validity domain of the EXCELL model which, in its primary formulation [*Capsoni et al.*, 1987b], is R_2 = 5 mm h^{-1}. *Awaka* [1989] and *Goldhirsh* [2000] arbitrarily extended the latter, assuming R_2 = 0.4 mm h^{-1}. In the present paper, R_2 will be taken equal to the rain rate threshold τ defined in

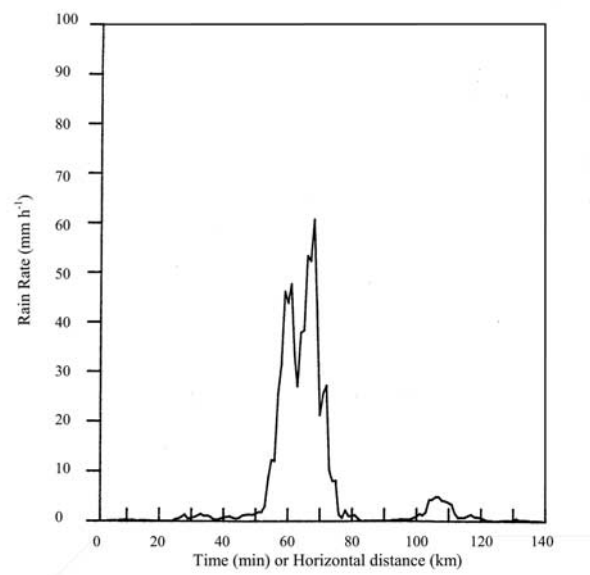

Figure 2. Temporal evolution (hyetograph) of the rain rate measured in the region of Niamey (Niger, Sahelian Africa) on 03 September 1988.

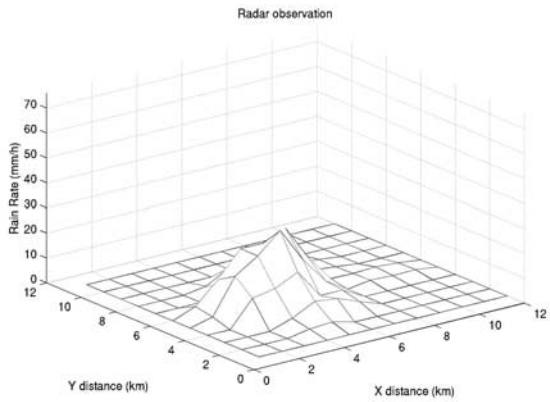

Figure 3a. Radar observation of a cell from the field of Bordeaux on 20/08/1996 at 08:00 UTC. The threshold is $\tau = 1$ mm h^{-1}. The peak rain rate measured by the radar is $R_{max} = 30.33$ mm h^{-1}.

Section 2, with the value $\tau = 1$ mm h^{-1}. This value is chosen rather arbitrarily to trade off between the rain cell with a significant rain activity and the stratiform shapeless background. So, in the following, the validity domain of EXCELL is supposed to be $R \geq R_2$ with $R_2 = 1$ mm h^{-1}.

[18] According to (2), a rain cell is thus fully described by the determination of the three parameters R_E, a_E , and b_E. These three parameters can be obtained, cell by cell, by forcing appropriate cell descriptors of integral nature to be the same for the radar observations and for the model [*Capsoni et al.*, 1987b]. For each cell identified from $\tau = R_2$, a set of three fit-forcing equations has to be solved (subscript r stands for radar measurement):

$$A_r = \int\int_{\Delta} dxdy = \pi a_E b_E \ln^2 \frac{R_E}{R_2}, \tag{3}$$

$$\overline{R_r} = \frac{1}{A_r}\int\int_{\Delta} R(x,y)dxdy = 2R_E\left[1 - \left(\frac{R_2}{R_E}\right)\left(1 + \ln\frac{R_E}{R_2}\right)\right] / \ln^2\left(\frac{R_E}{R_2}\right), \tag{4}$$

$$e_r = \frac{a_E}{b_E}. \tag{5}$$

Δ is the domain occupied by the rain cell in the horizontal plane with ordinate $R = R_2$. A_r, $\overline{R_r}$ and e_r are the area, the average rain rate, and the ellipticity of the cell, respectively, determined from the radar observations. Therefore, R_E is derived from the nonlinear equation (4). Its value minimises the error with respect to $\overline{R_r}$ while a_E and b_E are obtained from the exact (analytical) resolution of (3) and (5).

[19] EXCELL has been widely applied to study telecommunication link performance. However, it seems to present some shortcomings. First, from a conceptual point of view and as mentioned in Section 2, exponentially peaked distributions of rain rate are not observed in nature. Secondly, from a calculatory point of view, in the case of high values of $\overline{R}$, the associated value of R_E becomes unrealistic (cf. (4)). This is typically the case for rain cells generating heavy rain rates over significant areas (e.g., tropical rain cells but also deep convective cells at midlatitudes). *Capsoni et al.* [1987b], aware of this overestimation of R_E, did not consider it as a negative point, arguing for a compensation of the underestimation of radar measured peak values, R_{max} , due to the spatial averaging by the radar beam. Up to now, radar maxima of reflectivity in rain fields have never been shown to be significantly influenced by the radar resolution. In fact, the statistical study of the rain field characteristics from radar data does not show any dependency on the distance from the radar, neither for the rain rate parameters (notably R_{max}) nor for the rain cell size distribution [e.g., *Nzeukou and Sauvageot*, 2002] (among many others).

[20] Figures 3a and 3b show, as an example, the observation of a rain cell by the meteorological radar of Bordeaux (France) on 20/08/1996 at 08:00 UTC and its EXCELL modeling, respectively. The rain rate threshold is $\tau = R_2 = 1$ mm h^{-1}. Figure 3b underlines the limitation of the model with respect to parameter R_E. Indeed, if the radar cell shows a measured peak value of $R_{max} = 30.33$ mm h^{-1} (Figure 3a), its equivalent cell modeled by EXCELL has a peak rain rate $R_E = 75.11$ mm h^{-1}, which squares with an overestimation of about 147%. To overcome these drawbacks, an improvement of the modeling

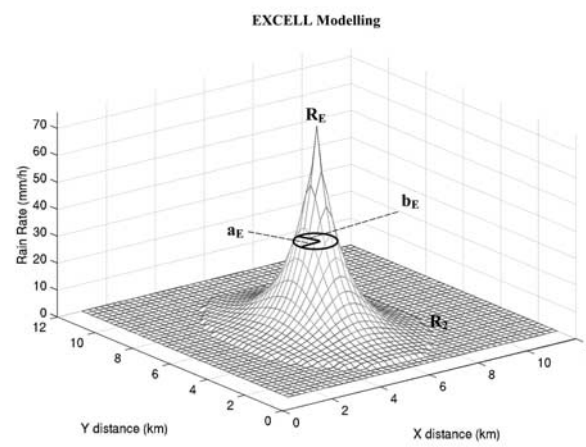

Figure 3b. EXCELL modeling of the cell observed by the radar of Bordeaux on 20/08/1996 at 08:00 UTC (Figure 3a). $R_2 = \tau = 1$ mm h^{-1}, (R_E, a_E, b_E) are the three parameters of the model. $R_E = 75.11$ mm h^{-1}.

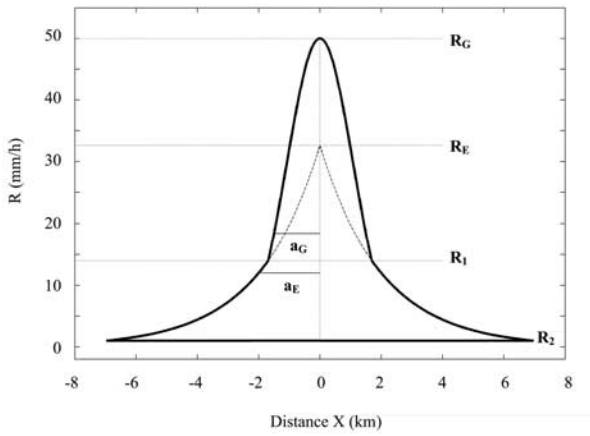

Figure 4. Representation in the vertical plane passing through the (Ox) axis of the HYCELL modeling. R_G and R_E are the gaussian and exponential peaks, respectively. a_G and a_E are the distances for which the rain rate R decreases by a factor 1/e with respect to R_G and R_E, respectively. R_1 delimits the zones of gaussian and exponential definition. $R_2 = 1$ mm h^{-1}.

of the rain rate horizontal distribution within the rain cells is proposed using a hybrid approach.

3.2. HYCELL Model

[21] As part of a hybrid modeling, the present study proposes to describe the rain rate horizontal distribution within the rain cells by combining an exponential component with a gaussian one (Figure 4), so that the analytical expression of the rain rate distribution becomes in the horizontal plane (Oxy):

$$\left.\begin{aligned} R(x,y) &= R_G \exp\left[-\left(\frac{x^2}{a_G^2}+\frac{y^2}{b_G^2}\right)\right] \quad \text{if } R \geq R_1, \\ &= R_E \exp\left[-\left(\frac{x^2}{a_E^2}+\frac{y^2}{b_E^2}\right)^{1/2}\right] \quad \text{if } R_2 \leq R < R_1. \end{aligned}\right\} \tag{6}$$

R_G, a_G and b_G define the gaussian component and are the peak rain rate and the distances along the axes (Ox) and (Oy) for which the rain rate decreases by a factor 1/e with respect to R_G , respectively. R_E, a_E and b_E define the exponential component with similar signification as for the gaussian component, as shown in Figure 4, where the hybrid modeling parameters are represented in a vertical plane passing by the Ox axis. R_1 separates the gaussian and exponential components. As the rain rate threshold considered in the present paper is $\tau = 1$ mm h^{-1}, the domain of definition of the hybrid model is $R \geq R_2$, with $R_2 = 1$ mm h^{-1}. This model will be termed the HYCELL model.

[22] As mentioned in Section 2, from a conceptual point of view, the gaussian component is assigned to the description of the convective area while the exponential component accounts for the stratiform spreading of the surrounding precipitation, so that excessively large values of R_G with respect to the peak rain rate R_{max} measured by the radar are avoided. The HYCELL model squares with the EXCELL model when $R_1 = R_G = R_E$. It is purely gaussian when $R_1 = R_2$.

[23] The EXCELL model definition lies on the computation of three parameters (R_E, a_E, b_E), but the description of the rain rate horizontal distribution within a rain cell by the HYCELL scheme requires the determination of seven parameters (R_G, a_G, b_G, R_E, a_E, b_E, R_1). The latter are obtained, cell by cell, by solving a set of five nonlinear fit-forcing equations completed by two continuity equations.

[24] The fit-forcing equations involve radar parameters of integral nature, which are therefore less space-resolution-dependent than a punctual parameter (as the rain rate maximum value, for example). Their analytical expressions can be derived from the HYCELL model definition (6) (cf. Appendix A) while their values are forced to those derived from the radar measurements. These integral parameters are the area A, the ellipticity e, the mean $\overline{R}$ and root mean square R_{rms} values of R, and the mean $\overline{G}$ and rms G_{rms} values of the modulus of the horizontal gradient of R. The fit-forcing equations of the HYCELL model are given below. The derivation of the equations is given in Appendix A. In these equations, subscript r indicates radar measurement and Δ is the domain occupied by the rain cell in the horizontal plane with ordinate $R = R_2$.

$$A_r = \int\int_\Delta dxdy = \pi a_G b_G \ln\frac{R_G}{R_1} + \pi a_E b_E \cdot\left(\ln^2\frac{R_E}{R_2} - \ln^2\frac{R_E}{R_1}\right). \tag{7}$$

$$A_r\overline{R_r} = \int\int_\Delta R(x,y)dxdy = \pi a_G b_G (R_G - R_1) + 2\pi a_E b_E\left[R_1\left(1+\ln\frac{R_E}{R_1}\right) - R_2\left(1+\ln\frac{R_E}{R_2}\right)\right]. \tag{8}$$

$$A_r\left(R_{rms}^2\right)_r = \int\int_\Delta R^2(x,y)dxdy = \frac{\pi}{2}a_G b_G\left(R_G^2 - R_1^2\right) + \frac{\pi}{2}a_E b_E\left[R_1^2\left(1+2\ln\frac{R_E}{R_1}\right) - R_2^2\left(1+2\ln\frac{R_E}{R_2}\right)\right]. \tag{9}$$

$$A_r\overline{G_r} = \int\int_\Delta G(x,y)dxdy = \cdot I_G\left[R_G\frac{\pi^{1/2}}{2}\mathrm{erf}\left(\ln^{1/2}\frac{R_G}{R_1}\right) - R_1\ln^{1/2}\frac{R_G}{R_1}\right] + I_E\left[R_1\left(1+\ln\frac{R_E}{R_1}\right) - R_2\left(1+\ln\frac{R_E}{R_2}\right)\right], \tag{10}$$

with $I_G = 4b_G E\left[\frac{\pi}{2}, \left(1-\frac{a_G^2}{b_G^2}\right)^{1/2}\right]$ and $I_E = 4b_E E\left[\frac{\pi}{2}, \left(1-\frac{a_E^2}{b_E^2}\right)^{1/2}\right]$ E is the elliptic integral of second kind and erf is the error function.

$$A_r\left(G_{rms}^2\right)_r = \int\int_\Delta G^2(x,y)dxdy = \frac{\pi}{2}\left(\frac{a_G}{b_G}+\frac{b_G}{a_G}\right) \cdot\left[R_G^2 - R_1^2\left(1+2\ln\frac{R_G}{R_1}\right)\right] + \frac{\pi}{4}\left(\frac{a_E}{b_E}+\frac{b_E}{a_E}\right) \cdot\left[R_1^2\left(1+2\ln\frac{R_E}{R_1}\right) - R_2^2\left(1+2\ln\frac{R_E}{R_2}\right)\right] \quad (11)$$

Two supplementary equations are derived from the continuity condition of the model for $R = R_1$:

$$a_G^2 \ln\frac{R_G}{R_1} = a_E^2 \ln^2\frac{R_E}{R_1}, \quad (12)$$

$$b_G^2 \ln\frac{R_G}{R_1} = b_E^2 \ln^2\frac{R_E}{R_1}. \quad (13)$$

If e is the ellipticity of the rain cell of elliptic shape, (12) and (13) give:

$$\frac{a_E}{b_E} = \frac{a_G}{b_G} = e_r. \quad (14)$$

Using (12), (13), and (14), (7) becomes:

$$A_r = \pi a_E b_E \ln^2\frac{R_E}{R_2} = \pi e_r b_E^2 \ln^2\frac{R_E}{R_2}. \quad (7')$$

From (7), (12), (13), and (14), equations (8), (9), (10), and (11) can be rewritten:

$$\overline{R_r} = \ln^{-2}\frac{R_E}{R_2}\left[\ln^2\frac{R_E}{R_1}\ln^{-1}\frac{R_G}{R_1}(R_G - R_1) + 2R_1\left(1+\ln\frac{R_E}{R_1}\right) - 2R_2\left(1+\ln\frac{R_E}{R_2}\right)\right], \quad (8')$$

$$2\left(R_{rms}^2\right)_r = \ln^{-2}\frac{R_E}{R_2}\left[\ln^{-1}\frac{R_G}{R_1}\ln^2\frac{R_E}{R_1}\cdot\left(R_G^2 - R_1^2\right) + R_1^2\left(1+2\ln\frac{R_E}{R_1}\right) - R_2^2\left(1+2\ln\frac{R_E}{R_2}\right)\right], \quad (9')$$

$$\overline{G_r} = \frac{4E\left[\frac{\pi}{2}, \left(1-e_r^2\right)^{1/2}\right]}{\left(A_r\pi e_r\right)^{1/2}\ln\frac{R_E}{R_2}}\left[R_G\frac{\pi^{1/2}}{2}\mathrm{erf}\left(\ln^{1/2}\frac{R_G}{R_1}\right)\ln\frac{R_E}{R_1} \cdot\ln^{-1/2}\frac{R_G}{R_1} + R_1 - R_2\left(1+\ln\frac{R_E}{R_2}\right)\right], \quad (10')$$

$$A_r\left(G_{rms}^2\right)_r = \frac{\pi}{2}\left(e_r+\frac{1}{e_r}\right)\left[R_G^2 - R_1^2\left(1+2\ln\frac{R_G}{R_1}\right) + \frac{R_1^2}{2}\left(1+2\ln\frac{R_E}{R_1}\right) - \frac{R_2^2}{2}\cdot\left(1+2\ln\frac{R_E}{R_2}\right)\right]. \quad (11')$$

[25] Therefore, the determination of R_G, R_1, and R_E involves the resolution of a nonlinear system of four equations with three unknowns. This system is, a priori, overdetermined. On the one hand, the value of R_G is greater than or equal to the peak rain rate R_{max} of the radar cell, defining a solution interval for R_G: $R_G \geq R_{max}$. On the other hand, R_1 varies from R_2 (purely gaussian model) to R_G (purely exponential model), giving an interval of definition for R_1: $R_2 \leq R_1 \leq R_G$. We proceed to a discretization of the solution space, and the optimal values of R_G, R_1, and R_E are determined numerically from (8′), (9′), (10′), and (11′) by the minimization of an error criterion ξ defined as the sum of the absolute values of the (normalized) errors with respect to $\overline{R_r}$, $(R_{rms})_r$, $\overline{G_r}$, and $(G_{rms})_r$, namely:

$$\xi = \left|\frac{\overline{R_H}}{\overline{R_r}} - 1\right| + \left|\frac{(R_{rms})_H}{(R_{rms})_r} - 1\right| + \left|\frac{\overline{G_H}}{\overline{G_r}} - 1\right| + \left|\frac{(G_{rms})_H}{(G_{rms})_r} - 1\right|, \quad (15)$$

where subscripts r and H refer to radar measurements and hybrid modeling, respectively.

[26] In the EXCELL model, the parameter R_E is obtained by solving (4), that is by minimizing the error with respect to $\overline{R_r}$. In the case of a purely exponential HYCELL model ($R_1 = R_G = R_E$), the determination of R_E results from the resolution of an equation system minimizing the error not only with respect $\overline{R_r}$, but also with respect to $(R_{rms})_r$, $\overline{G_r}$ and $(G_{rms})_r$. This methodological difference leads, even in the case of purely exponential cells, to improving the modeling of the rain rate distribution within the cells.

[27] One way to simplify the calculation is to remark that from (11'), in the case of a hybrid scheme ($R_2 < R_1 < R_G$), R_E can be expressed as a function of R_G, R_1, A_r, e_r, and $(G_{rms})_r$. This allows to reduce the number of unknown parameters from three to two while constraining the model to check (11'). Moreover, the optimal values of R_G and R_1 can be obtained numerically, from (7′), (8′) and (9′), by minimizing ξ, which now reduces to:

$$\xi = \left|\frac{\overline{R_H}}{\overline{R_r}} - 1\right| + \left|\frac{(R_{rms})_H}{(R_{rms})_r} - 1\right| + \left|\frac{\overline{G_H}}{\overline{G_r}} - 1\right|, \quad (15')$$

$(G_{rms})_H$ being now strictly equal to $(G_{rms})_r$ by definition of R_E from (11′). This methodological approach is the one used in the present paper.

[28] As for $\{a_G, b_G, a_E, b_E\}$, they are deduced analytically from (7'), (12), (13), (14). Three cases have to be considered according to the value of R_1:

[29] 1) $R_1 = R_2$ (purely gaussian model):

$$b_G^2 = \frac{A_r}{\pi e_r \ln\frac{R_G}{R_2}} \quad \text{and} \quad a_G = e_r b_G. \quad (16)$$

[30] 2) $R_1 = R_G = R_E$ (purely exponential model):

$$b_E^2 = \frac{A_r}{\pi e_r \ln^2 \frac{R_E}{R_2}} \quad \text{and} \quad a_E = e_r b_E. \tag{17}$$

[31] 3) $R_2 < R_1 < R_G$ (hybrid model):

$$b_E^2 = \frac{A_r}{\pi e_r \ln^2 \frac{R_E}{R_2}}, a_E = e_r b_E, \tag{18}$$

and

$$b_G^2 = \frac{b_E^2 \ln^2 \frac{R_E}{R_1}}{\ln \frac{R_G}{R_1}}, a_G = e_r b_G. \tag{19}$$

4. Tests

4.1. Radar Data

[32] The data come from two meteorological radar, one located at Bordeaux, in southwestern France, the other at Karlsruhe, in southwestern Germany. Though both sites are related to rain fields at midlatitude, the observations differ due to the climatic context, oceanic for Bordeaux and continental for Karlsruhe.

[33] The radar at Bordeaux, an S-band radar, is part of the French operational radar network managed by Météo France. It gives the spatial distribution of radar reflectivity in the form of Constant Altitude Plan Position Indicator (CAPPI) at 1.5 km above ground level, every 5 min. Measurements of reflectivities, corresponding to a contiguous pulse volume sampled each 500 m in range, were made over a circular area with a radius of 256 km. The CAPPI radar scans, in polar coordinates, were converted along a cartesian grid, with a uniform pixel size of 1×1 km^2. The data set contains 35286 CAPPIs, acquired from January to December 1996.

[34] The radar at Karlsruhe is a C-band radar performing a volume scan of the atmosphere. In the present paper the spatial distribution of radar reflectivity every 5 min in a horizontal plane, at 1.5 km above ground level is used. The radar images of the "surface rain intensity" (SRI) result from the interpolation of radar observations at various elevation angles. Here, the cartesian resolution is 0.5×0.5 km^2 and the domain observed is a circular area with radius of 120 km. The data set contains 38583 SRIs acquired from January to December 1999. The main technical characteristics of these two radars are given in Table 1.

[35] All the CAPPI or SRI images including ground clutter or melting layer echoes were removed from the data set so that the used radar data only refers to rain fields. At midlatitudes, the standard Z-R relation

$$Z = 300\ R^{1.5}, \tag{20}$$

with the radar reflectivity factor Z in mm^6 m^{-3} and the rain rate R in mm h^{-1}, is used to convert reflectivity fields into rain rate fields.

Table 1. Main Technical Characteristics of the Radars

	Bordeaux	Karlsruhe
Wavelength, cm	10 (S band)	5 (C band)
Peak power, kW	700	250
Pulse repetition frequency, Hz	250	250
3dB beam width. θ_{3dB}, deg.	1.75	0.98
Cartesian grid resolution	1×1 km^2	0.5×0.5 km^2
Observation radius, km	256	120

4.2. Rain Cell Identification

[36] For all available radar images from Bordeaux and Karlsruhe, each cell in the field is identified according to an automatic contouring procedure. The rain rate threshold τ is 1 mm h^{-1}. This value corresponds to a radar reflectivity of 25 dBZ using relation (20). Then, cell by cell, all the integral parameters required for the rain cell hybrid modeling are computed.

[37] First, from a morphological point of view, the rain cell area A_r is determined by counting the number of rainy pixels. Each cell is approximated by its equivalent ellipse whose geometrical features - major axis length, minor axis length and orientation angle - are computed, by minimization of the moments of inertia [*Féral et al.*, 2000], to finally obtain the cell ellipticity e_r.

[38] Secondly, as part of a textural approach, the maximum $(R_{max})_r$, mean $\overline{R}_r$, and rms $(R_{rms})_r$ values of the rain rate R, as well as the mean $\overline{G}_r$ and rms $(G_{rms})_r$ values of the modulus of the (numerical) gradient of R, are computed for each rain cell identified in the radar field at $\tau = 1$ mm h^{-1}. As mentioned in Section 3, subscript r stands for radar measurements.

[39] When doing this, it is important to keep in mind some of the radar limitations. The minimum detectable rain rate (MDRR) and the minimum cell size that can be resolved by the radar increase with distance (owing to the filtering by the pulse volume). The threshold considered in the present paper ($\tau = 1$ mm h^{-1}) is largely higher than the MDRR of the radars of Bordeaux and Karlsruhe at the farthest observed distance (about 12 dBZ at 100 km). The minimum cell size L_{min} resolved by the radars depends on the azimuthal resolution, that is on the maximum distance of observation d_{max} and on the 3dB beam width θ_{3dB} so that L_{min} must be greater than $d_{max} \times \theta_{3dB}$.

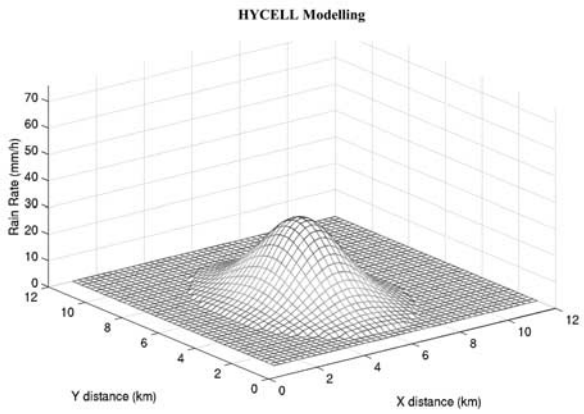

Figure 5. HYCELL modeling of the cell of Figure 3a, observed by the radar of Bordeaux on 20/08/1996 at 08:00 UTC. $R_2 = \tau = 1$ mm h^{-1}. $R_G = 30.33$ mm h^{-1}.

[40] Considering a maximum distance of observation d_{max} of 100 km at Bordeaux and 117 km at Karlsruhe, L_{min} is about 3 km and 2 km for the radars of Bordeaux and Karlsruhe, respectively. This left truncation leads to keep only the cells having an area A_r greater than 7 km^2 and 3 km^2 for Bordeaux and Karlsruhe, respectively. Moreover, all the rain cells which straddle the d_{max} frontier are removed from the data set.

[41] The maximum size L_{max} considered for the rain cells is about 20 km in equivalent diameter (300 km^2 in area). Beyond this size, of course, there are still rain structures; however, they are no longer rain cells but rather cell clusters, controlled by air motions, whose scale is larger than the rain cell. Anyway, the analysis of the radar data shows that cells larger than about 20 km in diameter are not numerous [*Mesnard and Sauvageot*, 2003]. If this method is applied, the number of rain cells finally identified by the radars of Bordeaux and Karlsruhe are 213112 and 701882, respectively.

4.3. Results

[42] For all the cells of Bordeaux and Karlsruhe, the seven parameters (R_G, a_G, b_G, R_E, a_E, b_E, R_1) defining the hybrid model have been computed according to the modeling methodology described in section 3.

[43] Figure 5 shows the HYCELL modeling of the rain cell, observed by the radar of Bordeaux, shown in Figure 3a. The qualitative improvement from the EXCELL model (Figure 3b) is obvious, notably with respect to R_G, which value no longer overestimates the radar measured peak rain rate R_{max} (R_G is even equal to R_{max} in that case).

[44] Figures 6a, 6b, and 6c, show three other examples of HYCELL modeling deduced from radar observations. The result of the modeling by EXCELL is also shown for comparison. The radar cells of cases a, b, and c are part of the same rain field, observed by the radar of Karlshrue on 02/06/1999 at 14:14 UTC. By construction, in all the cases, both HYCELL and EXCELL models reproduce exactly the area A_r and the ellipticity e_r of the radar cell with the additional constraint, for the HYCELL model, to reproduce exactly $(G_{rms})_r$.

[45] In cell 1, whatever the model considered, the peak rain rate measured by the radar is exactly reproduced by the peak values R_G and R_E of the HYCELL and EXCELL models, respectively. The relative error of HYCELL with respect to $\overline{R_r}$, $(R_{rms})_r$ and $\overline{G_r}$ is 2.93%, 0.08%, and 9.53%, respectively. When considering the EXCELL modeling, these values become 7.41%, 8.63%, and 16%, respectively. For $(G_{rms})_r$, the relative error of EXCELL is 25.03% (null error for HYCELL by construction). It is worth noting that, here, though the determination of the HYCELL parameters lies on the minimization of the functional (15′) - which involves not only $\overline{R_r}$ but also $(R_{rms})_r$ and $\overline{G_r}$ - the HYCELL model reproduces the mean rain rate $\overline{R_r}$ better than EXCELL.

[46] In cell 2, if HYCELL correctly accounts for the peak rain rate of the radar cell ($R_G = R_{max} = 175.50$ mm h^{-1}), EXCELL leads to $R_E = 240.73$ mm h^{-1}, which squares with an overestimation of 37%. EXCELL now describes optimally $\overline{R_r}$, whereas the relative error of HYCELL with respect to this parameter is 4.61%. When considering $(R_{rms})_r$, $\overline{G_r}$, and $(G_{rms})_r$, the relative errors of HYCELL (EXCELL, respectively) are 3.08% (3.58%), 4.54% (4.60%), and 0% (16.19%).

[47] In cell 3, both HYCELL and EXCELL models overestimate R_{max}, by about 211% for EXCELL but only 16% for HYCELL. Both models optimally reproduce $\overline{R_r}$. Now the relative errors of HYCELL (EXCELL) with respect to $(R_{rms})_r$, $\overline{G_r}$ and $(G_{rms})_r$ are 14.79% (36.69%), 4.61% (27.69%), and 0% (89.52%), respectively.

[48] As shown in Figure 6c (cell 3), the peak R_G of the cell modeled by a hybrid scheme is not necessarily equal to the peak rain rate $(R_{max})_r$ measured with the radar. Nevertheless, it does not display large values with respect to $(R_{max})_r$, as shown in Figures 7a and 7b, where the cumulative distribution function of $(R_{max})_r$, R_G (HYCELL peak rain rate), and R_E (EXCELL peak rain rate) are represented for the cells of Bordeaux and Karlsruhe, respectively.

[49] The usefulness of the hybrid modeling is all the more justified because the proportion of hybrid and gaussian cells is important with respect to the total population of modeled cells. Considering all the radar cells identified from Bordeaux and Karlsruhe at $\tau = R_2 = 1$ mm h^{-1}, the proportion of hybrid ($R_2 < R_1 < R_G$), purely exponential ($R_1 = R_G = R_E$), or purely gaussian ($R_2 = R_1$) cells, has been determined on a monthly and

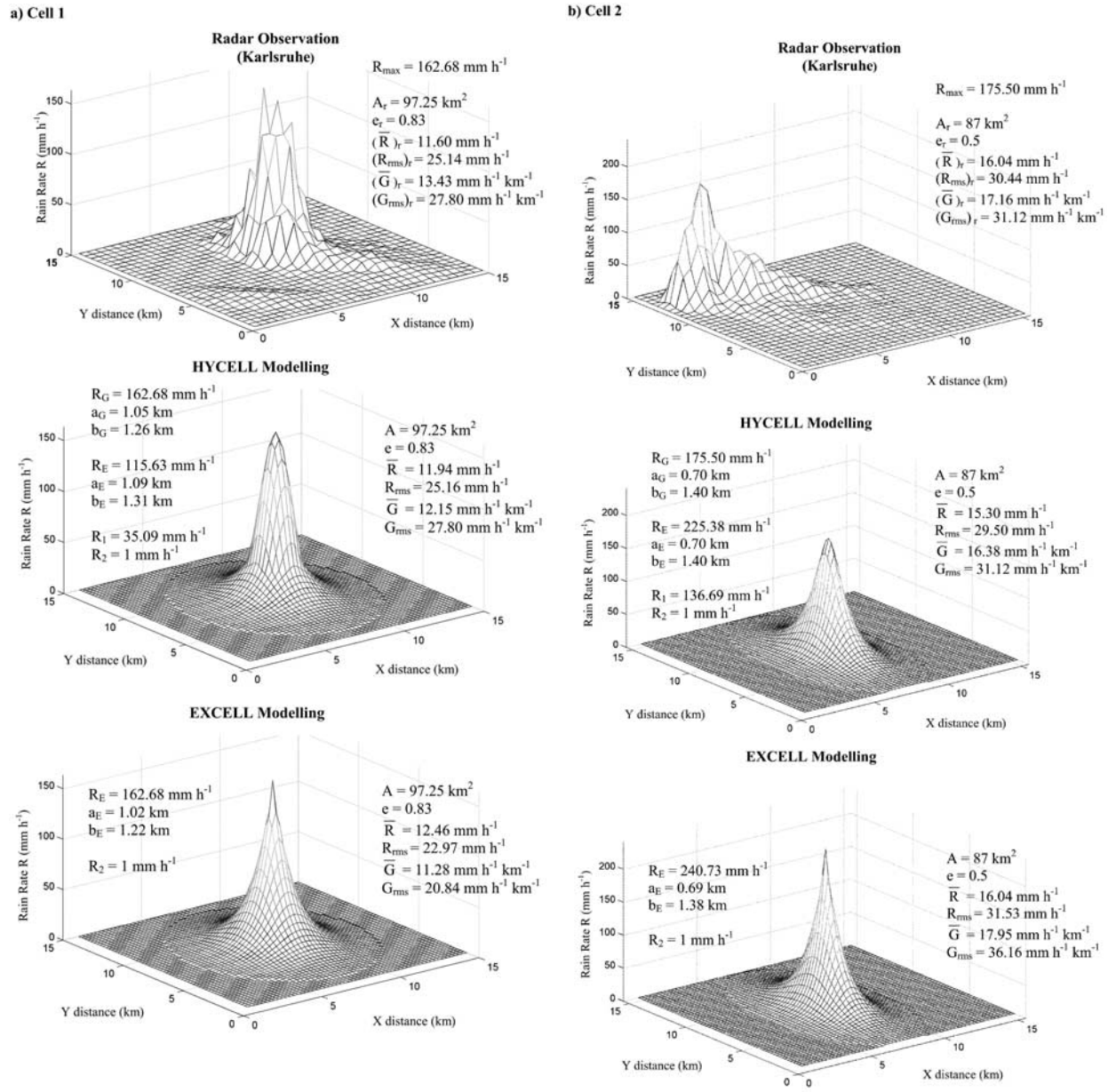

Figure 6. Examples of HYCELL and EXCELL modeling of three rain cells observed by the radar of Karlsruhe on 02/06/1999 at 14:14 UTC. The modeled cells are centered in the (X,Y) plane, their orientation is not forced to be the one of the radar cells.

annual basis. The results are shown in Table 2. What can be seen is that only 27 to 51% of the cells are purely exponential and thus are adapted to a modeling using the EXCELL scheme, while the HYCELL scheme is able to model all the cases. This fully justifies the usefulness of the turn to a hybrid modeling. Moreover, Table 2 shows that the proportion of hybrid cells is all the more important as convective months are considered - at least for the data set of Karlsruhe - leading to the conclusion that the description of the heavy convective rain cell organization does require the combination of a gaussian and an exponen-

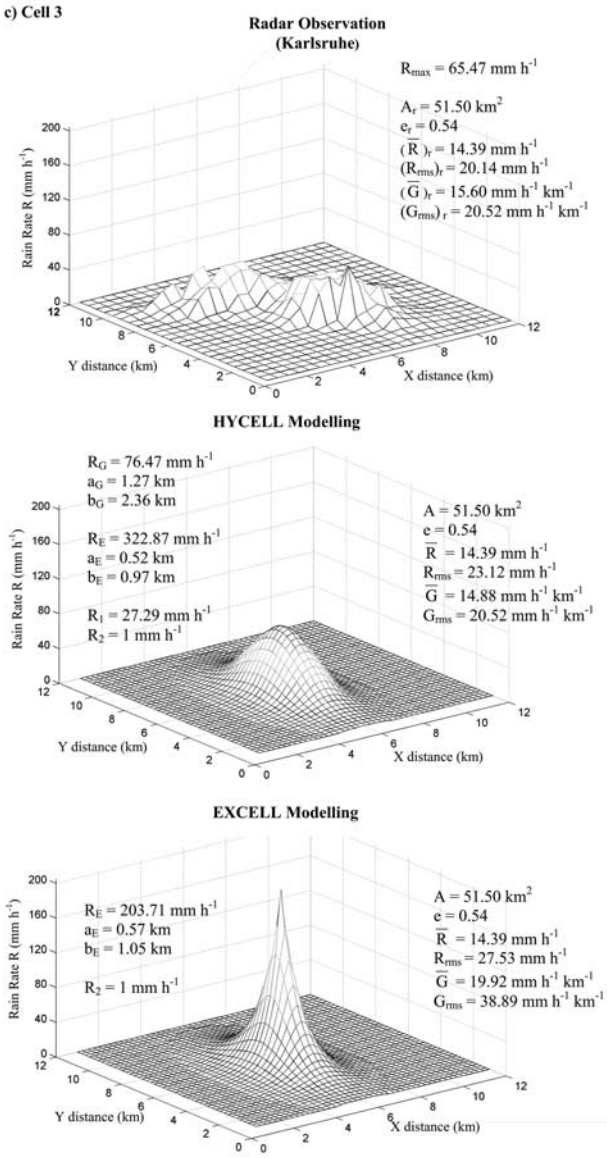

Figure 6. (continued)

tial component. If this trend is less pronounced for Bordeaux, it can be due to the oceanic influence on the climate of this region. In fact the atmospheric convection is more homogeneous over sea than over land, so that the maximum value of convection by-products is also smaller over sea than over land.

[50] For a quantitative assessment of the improvement of the HYCELL modeling with respect to the EXCELL one, for each rain cell, the ratio χ of the error of these two models with respect to the radar

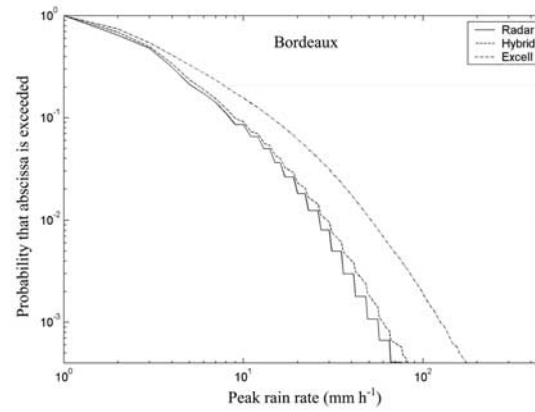

Figure 7a. Cumulative distribution function of the peak rain rate for the radar cells ($(R_{max})_r$, full line), for the cells modeled with EXCELL (R_E, dashed dot line), and for those modeled with the hybrid model (R_G, dot line). The results are derived from the radar data of Bordeaux.

integral parameters $\overline{R_r}$, $(R_{rms})_r$, $\overline{G_r}$ and $(G_{rms})_r$, has been computed, namely:

$$\chi = \frac{\mathrm{Error}_{\mathrm{EXCELL}}}{\mathrm{Error}_{\mathrm{HYCELL}}} = \frac{|\overline{R_{\mathrm{EXCELL}}} - \overline{R_r}| + |(R_{rms})_{\mathrm{EXCELL}} - (R_{rms})_r| + |\overline{G_{\mathrm{EXCELL}}} - \overline{G_r}| + |(G_{rms})_{\mathrm{EXCELL}} - (G_{rms})_r|}{|\overline{R_{\mathrm{HYCELL}}} - \overline{R_r}| + |(R_{rms})_{\mathrm{HYCELL}} - (R_{rms})_r| + |\overline{G_{\mathrm{HYCELL}}} - \overline{G_r}| + |(G_{rms})_{\mathrm{HYCELL}} - (G_{rms})_r|} \tag{21}$$

When the 213 112 cells of Bordeaux and the 701 882 cells of Karlsruhe are considered, it is found that, in average, $\overline{\chi}$ = 3.13 for Karlsruhe and $\overline{\chi}$ = 2.37 for Bordeaux.

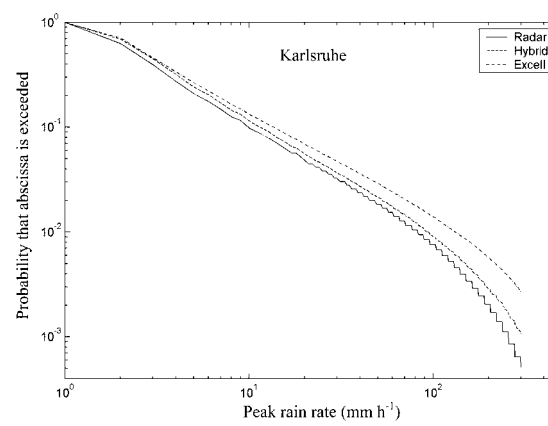

Figure 7b. Same as Figure 7a but for the radar data of Karlsruhe.

Table 2. Monthly and Total Percentage of Rain Cells Having a Hybrid Structure ($R_2 < R_1 < R_G$), and Purely Exponential ($R_1 = R_G = R_E$) or Purely Gaussian ($R_1 = R_2$) Structure, for Bordeaux (213 112 Cells) and Karlsruhe (701 882 Cells)

	Jan., %	Feb., %	March, %	April, %	May, %	June, %	July, %	Aug., %	Sept., %	Oct., %	Nov., %	Dec., %	Total, %
Bordeaux													
Purely Expo	45	39	43	40	40	43	47	43	43	42	46	51	42
Purely Gauss	8	7	9	11	11	10	11	14	12	10	8	6	10
Hybrid	47	54	48	49	49	47	42	43	45	48	46	43	48
Karlsruhe													
Purely Expo	41	39	38	28	32	29	27	28	33	29	48	51	34
Purely Gauss	2	2	2	2	2	2	3	2	2	2	4	4	2
Hybrid	57	59	60	70	66	69	70	70	65	69	48	45	64

[51] Figure 8 shows the monthly distribution of the mean value $\overline{\chi}$. As previously mentioned, it appears that the HYCELL modeling is all the better (with respect to EXCELL) as the rain cell convective organization is achieved. This suggests that the HYCELL model should be all the better (with respect to EXCELL) as we consider tropical cells showing a strong development of the convection. Anyway, be it for the rain cells of Bordeaux (oceanic climate) or Karlsruhe (continental climate), the HYCELL model proves efficient in describing the rain rate horizontal distribution within the rain cells.

[52] Another point of interest is the mean value $\overline{\chi}$ computed by distinguishing the hybrid cells from the purely exponential and purely gaussian cells. The results are shown in Table 3. Either for hybrid cells or for purely gaussian cells, $\overline{\chi}$ is about 3 to 4. For the purely exponential cells ($R_1 = R_G = R_E$), $\overline{\chi}$ is about 1.5. Thus, even in the case of a hybrid purely exponential scheme, HYCELL allows a more realistic modeling of the rain rate horizontal distribution within the cells than EXCELL. As explained in Section 3.2, this results from the methodological difference between the two models in the determination of R_E.

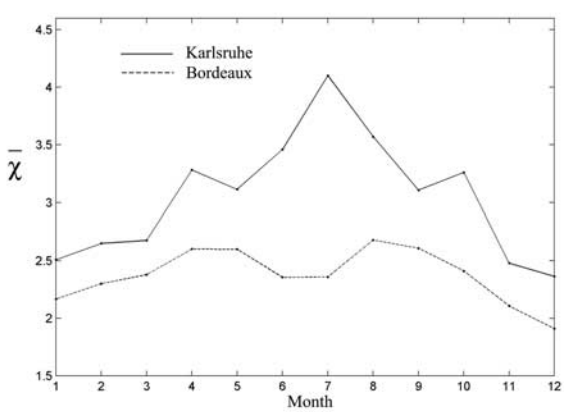

Figure 8. Monthly distribution of the mean value of the error ratio ($\overline{\chi}$).

5. Conclusion

[53] A new physical model of the rain cells named HYCELL has been presented. It allows to improve the description of the rain rate horizontal distribution within the cells by combining a gaussian function and an exponential one.

[54] The gaussian component accounts for the description of the rain rate distribution in the inner convective core of the cell, while the exponential component accounts for the surrounding stratiform component. In such a way, the mathematical definition of the hybrid (HYCELL) model provides the versatility necessary to the description of the internal structure of the real rain cells.

[55] The rain cell modeling by unimodal functions is justified by the fact that, firstly, the majority of the cells are single-peaked and, secondly, when they are not, the cells inside which several peaks of comparable intensity coexist are rather rare. Usually there is a main or dominant peak.

[56] The hybrid modeling of the rain cells requires the determination of seven parameters: R_G, a_G, b_G, R_E, a_E, b_E, and R_1. $\{R_G, a_G, b_G\}$ and $\{R_E, a_E, b_E\}$ define the

Table 3. Mean Value of the Error Ratio $\overline{\chi}$ for the Cells Having a Hybrid Structure ($R_2 < R_1 < R_G$), and Purely Gaussian ($R_2 = R_1$) or Purely Exponential ($R_1 = R_G = R_E$) Structure, for Bordeaux and Karlsruhe

	$\overline{\chi}$ (Bordeaux)	$\overline{\chi}$ (Karlsruhe)
Hybrid	3	3.32
Purely Gaussian	3.06	3.94
Purely Exponential	1.49	1.59

gaussian and exponential components, respectively, while R_1 delimits the zones of gaussian and exponential definition. Their values are obtained, cell by cell, by solving a set of five fit-forcing equations completed by two continuity equations. The fit-forcing equations involve radar parameters of integral nature. Their analytical expressions are derived from the hybrid model definition while their values are forced to be those obtained from radar measurements.

[57] According to the value of R_1, the hybrid scheme is able to model purely hybrid ($R_2 < R_1 < R_G$), purely gaussian ($R_1 = R_2$), and purely exponential cells ($R_1 = R_G = R_E$).

[58] When considering the 213112 cells of Bordeaux (southwestern France, oceanic climate) and the 701882 cells of Karlsruhe (southwestern Germany, continental climate), the results show that the new model enables the description of the rain rate horizontal distribution within the cells more accurately than the well-known EXCELL model, even in the case of cells having a purely exponential structure ($R_1 = R_G = R_E$). Moreover, the HYCELL model behaves still better (with respect to EXCELL) when rain cells with an achieved convective organization are considered. This results in an increasing proportion of hybrid cells ($R_2 < R_1 < R_G$) when convective months are considered. A significant advantage of HYCELL rests on its ability to describe with accuracy stratiform-like rain cells characterized by low peak rain rate and spreading on large area, which represents the most frequent situation at midlatitude and leads to strong attenuation at frequency higher than 15 GHz.

[59] The HYCELL modeling of rain cells, due to its ability to describe both their convective and stratiform components, should be an objective tool to evaluate and predict (from a statistical point of view) the temporal evolution of the rain cell internal structure, from their birth to their decay, by studying the temporal evolution of a limited number of parameters, the seven parameters which define the HYCELL model. Moreover, HYCELL should be a powerful tool to compute many propagation parameters. HYCELL is, for example, the basis of a new methodology of two-dimensional scene generating whose statistical properties follow the local climatology [*Féral et al.*, 2003].

Appendix A: Determination of the Analytical Expressions of A, $\overline{R}$, R_{rms}, $\overline{G}$, and G_{rms} From the HYCELL Model Definition (6)

[60] The mathematical definition of the HYCELL model is given by (6). As the model results from the combination of a gaussian function with an exponential one, the analytical expressions of the five integral parameters, namely A, $\overline{R}$, R_{rms}, $\overline{G}$, and G_{rms} (see section 3.2) have first to be determined independently for both functions.

A1. Gaussian Function

[61] Let R be the two-dimensional gaussian function of elliptic horizontal cross section ($a_G < b_G$), defined for $R \geq R_1$. In cartesian coordinates:

$$R(x,y) = R_G \exp\left[-\left(\frac{x^2}{a_G^2} + \frac{y^2}{b_G^2}\right)\right], \quad \text{for } R \geq R_1. \tag{A1}$$

The cartesian domain of definition Δ of R is thus:

$$\Delta = \left\{(x,y) \in \Re^2, \frac{x^2}{a_G^2} + \frac{y^2}{b_G^2} \leq \ln\frac{R_G}{R_1}\right\}. \tag{A2}$$

In polar coordinates, with $x = r\cos\omega$ and $y = r\sin\omega$. R can be rewritten:

$$R(r,\omega) = R_G \exp\left[-r^2\left(\frac{\cos^2\omega}{a_G^2} + \frac{\sin^2\omega}{b_G^2}\right)\right], \text{for } R \geq R_1. \tag{A3}$$

The domain of definition Δ becomes Δ_P ($a_G < b_G$):

$$\Delta_P = \left\{(r,\omega), \omega \in [0,2\pi], r \in \left[0, b_G \ln^{1/2}\frac{R_G}{R_1}\right], \right.$$
$$\left. r^2\left(\frac{\cos^2\omega}{a_G^2} + \frac{\sin^2\omega}{b_G^2}\right) \leq \ln\frac{R_G}{R_1}\right\}, \tag{A4}$$

and

$$r_1^2 = \ln\frac{R_G}{R_1} \Big/ \left(\frac{\cos^2\omega}{a_G^2} + \frac{\sin^2\omega}{b_G^2}\right). \tag{A5}$$

A1.1. Area A Over Which $R \geq R_1$

[62] Integrating with respect to r and considering (A5), gives:

$$A = \int\int_{\Delta} dxdy = \int\int_{\Delta_P} rdrd\omega = \int_0^{2\pi} d\omega \int_0^{r_1} rdr = \frac{1}{2}\ln\frac{R_G}{R_1}$$
$$\cdot \int_0^{2\pi} \frac{a_G^2 b_G^2}{b_G^2\cos^2\omega + a_G^2\sin^2\omega} d\omega. \tag{A6}$$

Now, it can be shown that:

$$\int_0^{2\pi} \frac{d\omega}{b_G^2 \cos^2\omega + a_G^2 \sin^2\omega} = \frac{2\pi}{a_G b_G}, \tag{A7}$$

thus (A6) can be rewritten:

$$A = \pi a_G b_G \ln \frac{R_G}{R_1}. \tag{A8}$$

A1.2. Mean Value of R(x, y) Over Δ

[63] Let $\overline{R}$ be the mean value of R(x, y) over Δ.

$$A\overline{R} = \int\int_\Delta R(x,y)dxdy = \int\int_{\Delta_P} R(r,\omega)rdrd\omega$$
$$= R_G \int_0^{2\pi} d\omega \int_0^{r_1} r \exp\left[-r^2\left(\frac{\cos^2\omega}{a_G^2} + \frac{\sin^2\omega}{b_G^2}\right)\right]dr. \tag{A9}$$

The integration with respect to r is straightforward. Considering (A5), (A9) becomes:

$$\int\int_\Delta R(x,y)dxdy = \frac{1}{2}(R_G - R_1) \cdot \int_0^{2\pi} \frac{a_G^2 b_G^2}{b_G^2 \cos^2\omega + a_G^2 \sin^2\omega} d\omega. \tag{A10}$$

(A7) finally gives:

$$A\overline{R} = \pi a_G b_G (R_G - R_1). \tag{A11}$$

A1.3. rms Value of R(x, y) Over Δ

[64] Let R_{rms} be the rms value of R(x, y) over Δ.

$$AR_{rms}^2 = \int\int_\Delta R^2(x,y)dxdy = \int\int_{\Delta_P} R^2(r,\omega)rdrd\omega$$
$$= R_G^2 \int_0^{2\pi} d\omega \int_0^{r_1} r \exp\left[-2r^2\left(\frac{\cos^2\omega}{a_G^2} + \frac{\sin^2\omega}{b_G^2}\right)\right]dr. \tag{A12}$$

Integrating with respect to r and considering (A5), (A12) becomes:

$$\int\int_\Delta R^2(x,y)dxdy = \frac{1}{4}(R_G^2 - R_1^2) \cdot \int_0^{2\pi} \frac{a_G^2 b_G^2}{b_G^2 \cos^2\omega + a_G^2 \sin^2\omega} d\omega. \tag{A13}$$

So that, from (A7):

$$AR_{rms}^2 = \frac{\pi}{2} a_G b_G (R_G^2 - R_1^2). \tag{A14}$$

A1.4. Mean Value of the Horizontal Gradient of R(x, y) Over Δ

[65] Let $\overline{G}$ be the mean value of the horizontal gradient of R(x, y) over Δ and G(x, y) the modulus of the horizontal gradient of R(x, y).

$$G(x,y) = 2\left[\frac{x^2}{a_G^4} + \frac{y^2}{b_G^4}\right]^{1/2} R_G \exp\left[-\left(\frac{x^2}{a_G^2} + \frac{y^2}{b_G^2}\right)\right], \quad \text{for } R \geq R_1. \tag{A15}$$

In polar coordinates, (A15) can be rewritten:

$$G(r,\omega) = 2r\left[\frac{\cos^2\omega}{a_G^4} + \frac{\sin^2\omega}{b_G^4}\right]^{1/2} \cdot R_G \exp\left[-r^2\left(\frac{\cos^2\omega}{a_G^2} + \frac{\sin^2\omega}{b_G^2}\right)\right], \quad \text{for } R \geq R_1. \tag{A16}$$

Thus,

$$A\overline{G} = \int\int_\Delta G(x,y)dxdy = \int\int_{\Delta_P} G(r,\omega)rdrd\omega$$
$$= 2R_G \int_0^{2\pi} \left[\frac{\cos^2\omega}{a_G^4} + \frac{\sin^2\omega}{b_G^4}\right]^{1/2} d\omega \cdot \int_0^{r_1} r^2 \exp\left[-r^2.\left(\frac{\cos^2\omega}{a_G^2} + \frac{\sin^2\omega}{b_G^2}\right)\right]dr. \tag{A17}$$

$$\text{Let } W = \left(\frac{\cos^2\omega}{a_G^2} + \frac{\sin^2\omega}{b_G^2}\right). \tag{A18}$$

In such conditions,

$$\int_0^{r_1} r^2 \exp\left[-r^2\left(\frac{\cos^2\omega}{a_G^2} + \frac{\sin^2\omega}{b_G^2}\right)\right]dr = \int_0^{r_1} r^2 \exp\left(-r^2 W\right)dr, \tag{A19}$$

and, integrating by parts:

$$\int_0^{r_1} r^2 \exp\left[-r^2\left(\frac{\cos^2\omega}{a_G^2} + \frac{\sin^2\omega}{b_G^2}\right)\right]dr = -\frac{r_1}{2W}\exp\left(-r_1^2 W\right) + \frac{1}{2W}\int_0^{r_1} \exp(-r^2 W)dr. \tag{A20}$$

The substitution $u = W^{1/2}r$ yields:

$$\int_0^{r_1} r^2 \exp\left[-r^2\left(\frac{\cos^2\omega}{a_G^2}+\frac{\sin^2\omega}{b_G^2}\right)\right]dr = -\frac{r_1}{2W}\exp\left(-r_1^2 W\right) + \frac{1}{2W^{3/2}}\int_0^{r_1 W^{1/2}} \exp(-u^2)du. \quad (A21)$$

Introducing the error function erf,

$$\mathrm{erf}(x) = 2\pi^{-1/2}\int_0^x \exp(-t^2)dt, \quad (A22)$$

leads to:

$$\int_0^{r_1} r^2 \exp\left[-r^2\left(\frac{\cos^2\omega}{a_G^2}+\frac{\sin^2\omega}{b_G^2}\right)\right]dr = -\frac{r_1}{2W}\exp\left(-r_1^2 W\right) + \frac{\pi^{1/2}}{4W^{3/2}}\mathrm{erf}(r_1 W^{1/2}). \quad (A23)$$

From (A5) and (A18),

$$r_1^2 = \ln\frac{R_G}{R_1}/W. \quad (A24)$$

One can deduce:

$$\int_0^{r_1} r^2 \exp\left[-r^2\left(\frac{\cos^2\omega}{a_G^2}+\frac{\sin^2\omega}{b_G^2}\right)\right]dr = W^{-3/2}\left[\frac{\pi^{1/2}}{4}\mathrm{erf}\left(\ln^{1/2}\frac{R_G}{R_1}\right)-\frac{R_1}{2R_G}\ln^{1/2}\frac{R_G}{R_1}\right], \quad (A25)$$

so that:

$$\int\int_\Delta G(x,y)dxdy = \left[\frac{R_G\pi^{1/2}}{2}\mathrm{erf}\left(\ln^{1/2}\frac{R_G}{R_1}\right)-R_1\ln^{1/2}\frac{R_G}{R_1}\right]a_G b_G \cdot \int_0^{2\pi}\frac{\left(b_G^4\cos^2\omega+a_G^4\sin^2\omega\right)^{1/2}}{\left(b_G^2\cos^2\omega+a_G^2\sin^2\omega\right)^{3/2}}d\omega. \quad (A26)$$

From the properties of the functions sin and cos, (A26) can be rewritten:

$$\int\int_\Delta G(x,y)dxdy = \left[\frac{R_G\pi^{1/2}}{2}\mathrm{erf}\left(\ln^{1/2}\frac{R_G}{R_1}\right)-R_1\ln^{1/2}\frac{R_G}{R_1}\right]4a_G \cdot \int_0^{\pi/2}\frac{\left(1-q^2\sin^2\omega\right)^{1/2}}{\left(1-p^2\sin^2\omega\right)^{3/2}}d\omega, \quad (A27)$$

where

$$q^2 = \frac{b_G^4-a_G^4}{b_G^4} \text{ and } p^2 = \frac{b_G^2-a_G^2}{b_G^2}. \quad (A28)$$

As a_G and b_G are the minor and major axes for which R decreases by a factor 1/e with respect to R_G, respectively,

$$a_G < b_G \text{ and } 0 < p^2 < q^2 < 1. \quad (A29)$$

Under the condition (A29), it can be shown that,

$$\int_0^{\pi/2}\frac{\left(1-q^2\sin^2\omega\right)^{1/2}}{\left(1-p^2\sin^2\omega\right)^{3/2}}d\omega = \frac{1}{(1-p^2)^{1/2}}E\left(\frac{\pi}{2},K\right), \quad (A30)$$

where $K^2 = \frac{q^2-p^2}{1-p^2}$ and $E\left(\frac{\pi}{2},K\right)$ is the elliptic integral of second kind, namely:

$$E\left(\frac{\pi}{2},K\right) = \int_0^{\pi/2}\left(1-K^2\sin^2\omega\right)^{1/2}d\omega. \quad (A31)$$

Therefore,

$$a_G b_G\int_0^{2\pi}\frac{\left(b_G^4\cos^2\omega+a_G^4\sin^2\omega\right)^{1/2}}{\left(b_G^2\cos^2\omega+a_G^2\sin^2\omega\right)^{3/2}}d\omega = 4b_G E\left[\frac{\pi}{2},\left(1-\frac{a_G^2}{b_G^2}\right)^{1/2}\right], \quad (A32)$$

and (A26) finally becomes,

$$A\overline{G} = 4b_G E\left[\frac{\pi}{2},\left(1-\frac{a_G^2}{b_G^2}\right)^{1/2}\right] \cdot \left[\frac{R_G\pi^{1/2}}{2}\mathrm{erf}\left(\ln^{1/2}\frac{R_G}{R_1}\right)-R_1\ln^{1/2}\frac{R_G}{R_1}\right]. \quad (A33)$$

A1.5. rms Value of the Horizontal Gradient of R(x, y) Over Δ

[66] Let G_{rms} be the rms value of the horizontal gradient of R(x, y) over Δ.

$$AG_{rms}^2 = \int\int_{\Delta} G^2(x,y)dxdy = \int\int_{\Delta_P} G^2(r,\omega)rdrd\omega$$
$$= 4R_G^2 \int_0^{2\pi} \left(\frac{\cos^2\omega}{a_G^4} + \frac{\sin^2\omega}{b_G^4}\right) d\omega \int_0^{r_1} r^3 \exp$$
$$\cdot\left[-2r^2\left(\frac{\cos^2\omega}{a_G^2} + \frac{\sin^2\omega}{b_G^2}\right)\right]dr. \quad \text{(A34)}$$

Let

$$W_1 = \left(\frac{\cos^2\omega}{a_G^4} + \frac{\sin^2\omega}{b_G^4}\right) \text{ and, as before,}$$
$$W = \left(\frac{\cos^2\omega}{a_G^2} + \frac{\sin^2\omega}{b_G^2}\right). \quad \text{(A35)}$$

In such conditions,

$$\int\int_{\Delta} G^2(x,y)dxdy = 4R_G^2 \int_0^{2\pi} W_1 d\omega \int_0^{r_1} r^3 \exp\left(-2r^2 W\right)dr. \quad \text{(A36)}$$

The integration with respect to r is straightforward and (A5) leads to:

$$\int\int_{\Delta} G^2(x,y)dxdy = \frac{1}{2}\left[R_G^2 - R_1^2\left(1 + 2\ln\frac{R_G}{R_1}\right)\right]$$
$$\cdot \int_0^{2\pi} \frac{W_1}{W^2} d\omega. \quad \text{(A37)}$$

Now,

$$\int_0^{2\pi} \frac{W_1}{W^2} d\omega = \int_0^{2\pi} \frac{b_G^4\cos^2\omega + a_G^4\sin^2\omega}{\left(b_G^2\cos^2\omega + a_G^2\sin^2\omega\right)^2} d\omega$$
$$= \pi\left(\frac{b_G}{a_G} + \frac{a_G}{b_G}\right). \quad \text{(A38)}$$

Therefore,

$$AG_{rms}^2 = \frac{\pi}{2}\left(\frac{b_G}{a_G} + \frac{a_G}{b_G}\right)\left[R_G^2 - R_1^2\left(1 + 2\ln\frac{R_G}{R_1}\right)\right]. \quad \text{(A39)}$$

A2. Exponential Function

[67] Now, let R be the two-dimensional exponential function of elliptic horizontal cross section ($a_E < b_E$), defined for $R \geq R_2$. In cartesian coordinates:

$$R(x,y) = R_E \exp\left[-\left(\frac{x^2}{a_E^2} + \frac{y^2}{b_E^2}\right)^{1/2}\right] \text{ for } R \geq R_2. \quad \text{(A40)}$$

The cartesian domain of definition Δ of R is now:

$$\Delta = \left\{(x,y) \in \Re^2, \frac{x^2}{a_E^2} + \frac{y^2}{b_E^2} \leq \ln^2\frac{R_E}{R_2}\right\}. \quad \text{(A41)}$$

In polar coordinates (x = rcosω and y = rsinω), R can be rewritten:

$$R(r,\omega) = R_E \exp\left[-r\left(\frac{\cos^2\omega}{a_E^2} + \frac{\sin^2\omega}{b_E^2}\right)^{1/2}\right] \text{ for } R \geq R_2 \quad \text{(A42)}$$

and the domain of definition Δ becomes Δ_P ($a_E < b_E$):

$$\Delta_P = \left\{(r,\omega), \omega \in [0,2\pi], r \in \left[0, b_E \ln\frac{R_E}{R_2}\right],\right.$$
$$\left. r^2\left(\frac{\cos^2\omega}{a_E^2} + \frac{\sin^2\omega}{b_E^2}\right) \leq \ln^2\frac{R_E}{R_2}\right\}, \quad \text{(A43)}$$

and

$$r_2^2 = \ln^2\frac{R_E}{R_2} \Big/ \left(\frac{\cos^2\omega}{a_E^2} + \frac{\sin^2\omega}{b_E^2}\right). \quad \text{(A44)}$$

A2.1. Area A Over Which R ≥ R_2

[68] Integrating with respect to r and considering (A44) and (A7), gives:

$$A = \int\int_{\Delta} dxdy = \int\int_{\Delta_P} rdrd\omega = \int_0^{2\pi} d\omega \int_0^{r_2} rdr$$
$$= \pi a_E b_E \ln^2\frac{R_E}{R_2}. \quad \text{(A45)}$$

A2.2. Mean Value of R(x, y) Over Δ

[69] Let $\overline{R}$ be the mean value of R(x, y) over Δ.

$$A\overline{R} = \int\int_{\Delta} R(x,y)dxdy = \int\int_{\Delta_P} R(r,\omega)rdrd\omega$$
$$= R_E \int_0^{2\pi} d\omega \int_0^{r_2} r\exp\left[-r.\left(\frac{\cos^2\omega}{a_E^2} + \frac{\sin^2\omega}{b_E^2}\right)^{1/2}\right]dr. \quad \text{(A46)}$$

The integration with respect to r is straightforward and (A44) leads to:

$$\int\int_{\Delta} R(x,y)dxdy = \left[R_E - R_2\left(1+\ln\frac{R_E}{R_2}\right)\right] \cdot \int_0^{2\pi} \frac{a_E^2 b_E^2}{b_E^2\cos^2\omega + a_E^2\sin^2\omega}d\omega. \tag{A47}$$

From (A7), (A47) becomes:

$$A\overline{R} = 2\pi a_E b_E\left[R_E - R_2\left(1+\ln\frac{R_E}{R_2}\right)\right]. \tag{A48}$$

A2.3. rms Value of R(x, y) Over Δ

[70] Let R_{rms} be the rms value of R(x, y) over Δ.

$$AR_{rms}^2 = \int\int_{\Delta} R^2(x,y)dxdy = \int\int_{\Delta_P} R^2(r,\omega)rdrd\omega = R_E^2\int_0^{2\pi} d\omega\int_0^{r_2} r\ \exp\left[-2r\left(\frac{\cos^2\omega}{a_E^2}+\frac{\sin^2\omega}{b_E^2}\right)^{1/2}\right]dr. \tag{A49}$$

Integrating with respect to dr and considering (A44), (A49) can be rewritten:

$$\int\int_{\Delta} R^2(x,y)dxdy = \frac{1}{4}\left[R_E^2 - R_2^2\left(1+2\ln\frac{R_E}{R_2}\right)\right] \cdot \int_0^{2\pi}\frac{a_E^2 b_E^2}{b_E^2\cos^2\omega + a_E^2\sin^2\omega}d\omega, \tag{A50}$$

so that, from (A7):

$$AR_{rms}^2 = \frac{\pi}{2}a_E b_E\left[R_E^2 - R_2^2\left(1+2\ln\frac{R_E}{R_2}\right)\right]. \tag{A51}$$

A2.4. Mean Value of the Horizontal Gradient of R(x, y) Over Δ

[71] Let $\overline{G}$ be the mean value of the horizontal gradient of R(x, y) over Δ and G(x, y) the modulus of the horizontal gradient of R(x, y).

$$G(x,y) = \left(\frac{b_E^4x^2 + a_E^4y^2}{b_E^2x^2 + a_E^2y^2}\right)^{1/2}\frac{R_E}{a_E b_E}\exp\left[-\left(\frac{x^2}{a_E^2}+\frac{y^2}{b_E^2}\right)^{1/2}\right], \quad \text{for } R \geq R_2. \tag{A52}$$

In polar coordinates:

$$G(r,w) = \left(\frac{b_E^4\cos^2\omega + a_E^4\sin^2\omega}{b_E^2\cos^2\omega + a_E^2\sin^2\omega}\right)^{1/2}\frac{R_E}{a_E b_E} \cdot \exp\left[-r\left(\frac{\cos^2\omega}{a_E^2}+\frac{\sin^2\omega}{b_E^2}\right)^{1/2}\right], \text{ for } R \geq R_2. \tag{A53}$$

In such conditions,

$$A\overline{G} = \int\int_{\Delta} G(x,y)dxdy = \int\int_{\Delta_P} G(r,\omega)rdrd\omega = \frac{R_E}{a_E b_E}\int_0^{2\pi}\left(\frac{b_E^4\cos^2\omega + a_E^4\sin^2\omega}{b_E^2\cos^2\omega + a_E^2\sin^2\omega}\right)^{1/2}d\omega \cdot \int_0^{r_2} r\exp\left[-r\left(\frac{\cos^2\omega}{a_E^2}+\frac{\sin^2\omega}{b_E^2}\right)^{1/2}\right]dr. \tag{A54}$$

Considering (A44), the integration with respect to r leads to:

$$\int\int_{\Delta} G(x,y)dxdy = a_E b_E\left[R_E - R_2.\left(1+\ln\frac{R_E}{R_2}\right)\right]\int_0^{2\pi} \cdot \frac{\left(b_E^4\cos^2\omega + a_E^4\sin^2\omega\right)^{1/2}}{\left(b_E^2\cos^2\omega + a_E^2\sin^2\omega\right)^{3/2}}d\omega. \tag{A55}$$

a_E and b_E are, respectively, the minor and major axes for which R decreases by a factor 1/e with respect to R_E, so that $a_E < b_E$.

[72] From (A32) and under the condition (A29) now verified by a_E and b_E:

$$a_E b_E\int_0^{2\pi}\frac{\left(b_E^4\cos^2\omega + a_E^4\sin^2\omega\right)^{1/2}}{\left(b_E^2\cos^2\omega + a_E^2\sin^2\omega\right)^{3/2}}d\omega = 4b_E E\left[\frac{\pi}{2},\left(1-\frac{a_E^2}{b_E^2}\right)^{1/2}\right], \tag{A56}$$

where E is the elliptic integral of second kind introduced previously. Finally,

$$A\overline{G} = 4b_E E\left[\frac{\pi}{2},\left(1-\frac{a_E^2}{b_E^2}\right)^{1/2}\right]\left[R_E - R_2\left(1+\ln\frac{R_E}{R_2}\right)\right]. \tag{A57}$$

A2.5. rms Value of the Horizontal Gradient of R(x, y) Over Δ

[73] Let G_{rms} be the rms value of the horizontal gradient of R(x, y) over Δ.

$$AG_{rms}^2 = \int\int_{\Delta} G^2(x,y)dxdy = \int\int_{\Delta_P} G^2(r,\omega)rdrd\omega$$
$$= \frac{R_E^2}{a_E^2 b_E^2}\int_0^{2\pi}\left(\frac{b_E^4\cos^2\omega + a_E^4\sin^2\omega}{b_E^2\cos^2\omega + a_E^2\sin^2\omega}\right)d\omega$$
$$\cdot\int_0^{r_2} r\exp\left[-2r\left(\frac{\cos^2\omega}{a_G^2}+\frac{\sin^2\omega}{b_G^2}\right)^{1/2}\right]dr. \quad (A58)$$

Considering (A44), the integration with respect to r leads to:

$$\int\int_{\Delta} G^2(x,y)dxdy = \frac{1}{4}\left[R_E^2 - R_2^2.\left(1+2\ln\frac{R_E}{R_2}\right)\right]$$
$$\cdot\int_0^{2\pi}\frac{b_E^4\cos^2\omega + a_E^4\sin^2\omega}{\left(b_E^2\cos^2\omega + a_E^2\sin^2\omega\right)^2}d\omega, \quad (A59)$$

and from (A38),

$$AG_{rms}^2 = \frac{\pi}{4}\left(\frac{b_E}{a_E}+\frac{a_E}{b_E}\right)\left[R_E^2 - R_2^2\left(1+2\ln\frac{R_E}{R_2}\right)\right]. \quad (A60)$$

A3. Hybrid Model

[74] Let R be the two-dimensional function defined, according to the hybrid model (6), by:

$$\left.\begin{aligned} R(x,y) &= R_G\exp\left[-\left(\frac{x^2}{a_G^2}+\frac{y^2}{b_G^2}\right)\right], && \text{if } R \geq R_1,\\ &= R_E\exp\left[-\left(\frac{x^2}{a_E^2}+\frac{y^2}{b_E^2}\right)^{1/2}\right], && \text{if } R_2 \leq R < R_1.\end{aligned}\right\} \quad (A61)$$

The analytical expressions of the five integral parameters, namely A, $\overline{R}$, R_{rms}, $\overline{G}$, and G_{rms} can be deduced from the results obtained in the two previous sections. From (A61), the domain of definition Δ of R can be simply expressed as the area in the horizontal plane where R(x, y) ≥ R_2.

A3.1. Area A Over Which R ≥ R_2

[75] From (A8) and (A45):

$$A = \iint_{\Delta} dxdy = \pi a_G b_G \ln\frac{R_G}{R_1} + \pi a_E b_E\left(\ln^2\frac{R_E}{R_2} - \ln^2\frac{R_E}{R_1}\right). \quad (A62)$$

Due to the continuity equations (12) and (13) for R = R_1, (A62) reduces to:

$$A = \pi a_E b_E \ln^2\frac{R_E}{R_2}. \quad (A63)$$

A3.2. Mean Value of R(x, y) Over Δ

[76] Let $\overline{R}$ be the mean value of R(x, y) over Δ. From (A11) and (A48):

$$A\overline{R} = \int\int_{\Delta} R(x,y)dxdy = \pi a_G b_G(R_G - R_1)$$
$$+ 2\pi a_E b_E\left[R_E - R_2\left(1+\ln\frac{R_E}{R_2}\right)\right]$$
$$- 2\pi a_E b_E\left[R_E - R_1\left(1+\ln\frac{R_E}{R_1}\right)\right] = \pi a_G b_G(R_G - R_1)$$
$$+ 2\pi a_E b_E\left[R_1\left(1+\ln\frac{R_E}{R_1}\right) - R_2\left(1+\ln\frac{R_E}{R_2}\right)\right]. \quad (A64)$$

A3.3. rms Value of R(x, y) Over Δ

[77] Let R_{rms} be the rms value of R(x, y) over Δ. From (A14) and (A51):

$$AR_{rms}^2 = \int\int_{\Delta} R^2(x,y)dxdy = \frac{\pi}{2}a_G b_G\left(R_G^2 - R_1^2\right)$$
$$+\frac{\pi}{2}a_E b_E\left[R_E^2 - R_2^2\left(1+2\ln\frac{R_E}{R_2}\right)\right]$$
$$-\frac{\pi}{2}a_E b_E\left[R_E^2 - R_1^2\left(1+2\ln\frac{R_E}{R_1}\right)\right]$$
$$= \frac{\pi}{2}a_G b_G\left(R_G^2 - R_1^2\right) + \frac{\pi}{2}a_E b_E$$
$$\cdot\left[R_1^2\left(1+2\ln\frac{R_E}{R_1}\right) - R_2^2\left(1+2\ln\frac{R_E}{R_2}\right)\right]. \quad (A65)$$

A3.4. Mean Value of the Horizontal Gradient of R(x, y) Over Δ

[78] Let $\overline{G}$ be the mean value of the horizontal gradient of R(x, y) over Δ and G(x, y) the modulus of the horizontal gradient of R(x, y). From (A33) and (A57):

$$A\overline{G} = \int\int_{\Delta} G(x,y)dxdy$$
$$= I_G\left[R_G\frac{\pi^{1/2}}{2}\operatorname{erf}\left(\ln^{1/2}\frac{R_G}{R_1}\right) - R_1\ln^{1/2}\frac{R_G}{R_1}\right]$$
$$+ I_E\left[R_1\left(1+\ln\frac{R_E}{R_1}\right) - R_2\left(1+\ln\frac{R_E}{R_2}\right)\right], \quad (A66)$$

where $I_G = 4b_G E\left[\frac{\pi}{2}, \left(1 - \frac{a_G^2}{b_G^2}\right)^{1/2}\right]$ and $I_E = 4b_E E\left[\frac{\pi}{2}, \left(1 - \frac{a_E^2}{b_E^2}\right)^{1/2}\right]$.

Importantly (14) gives:

$$E\left[\frac{\pi}{2}, \left(1 - \frac{a_G^2}{b_G^2}\right)^{1/2}\right] = E\left[\frac{\pi}{2}, \left(1 - \frac{a_E^2}{b_E^2}\right)^{1/2}\right].$$

A3.5. rms Value of the Horizontal Gradient of R(x, y) Over Δ

[79] Let G_{rms} be the rms value of the horizontal gradient of R(x, y) over Δ. From (A39) and (A60):

$$AG_{rms}^2 = \int\int_{\Delta} G^2(x,y)dxdy = \frac{\pi}{2}\left(\frac{b_G}{a_G} + \frac{a_G}{b_G}\right) \cdot \left[R_G^2 - R_1^2\left(1 + 2\ln\frac{R_G}{R_1}\right)\right] + \frac{\pi}{4}\left(\frac{b_E}{a_E} + \frac{a_E}{b_E}\right) \cdot \left[R_1^2\left(1 + 2\ln\frac{R_E}{R_1}\right) - R_2^2\left(1 + 2\ln\frac{R_E}{R_2}\right)\right]. \quad (A67)$$

Moreover, from (14), (A67) reduces to:

$$AG_{rms}^2 = \frac{\pi}{2}\left(\frac{b_G}{a_G} + \frac{a_G}{b_G}\right) \cdot \left[R_G^2 - R_1^2\left(1 + 2\ln\frac{R_G}{R_1}\right) + \frac{R_1^2}{2}\left(1 + 2\ln\frac{R_E}{R_1}\right) - \frac{R_2^2}{2}\left(1 + 2\ln\frac{R_E}{R_2}\right)\right]. \quad (A68)$$

[80] **Acknowledgments.** The authors are very grateful to Météo-France and to Dr. Jan Handwerker, from the Institut für Meteorologie und Klimaforschung of Karlsruhe, for providing without fee the radar data from Bordeaux and Karlsruhe, respectively.

References

Awaka, J., A three-dimensional rain cell model for the study of interference due to hydrometeor scattering, *J. Commun. Res. Lab.*, *36*(147), 13–44, 1989.

Capsoni, C., F. Fedi, and A. Paraboni, A comprehensive meteorologically oriented methodology for the prediction of wave propagation parameters in telecommunication applications beyond 10 GHz, *Radio Sci.*, *22*(3), 387–393, 1987a.

Capsoni, C., F. Fedi, C. Magistroni, A. Paraboni, and A. Pawlina, Data and theory for a new model of the horizontal structure of rain cells for propagation applications, *Radio Sci.*, *22*(3), 395–404, 1987b.

Castanet, L., J. Lemorton, T. Konefal, A. Shukla, P. Watson, and C. Wrench, Comparison of combined propagation models for predicting loss in low-availability systems that operate in the 20 GHz to 50 GHz frequency range, *Int. J. Satell. Commun.*, *19*(3), 317–334, 2001.

Castanet, L., D. Mertens, and M. Bousquet, Simulation of the performance of a Ka-band VSAT videoconferencing system with uplink power control and data rate reduction to mitigate atmospheric propagation effects, *Int. J. Satell. Commun.*, *20*(4), 231–249, 2002a.

Castanet, L., M. Bousquet, M. Filip, P. Gallois, B. Gremont, L. De Haro, J. Lemorton, A. Paraboni, and M. Schnell, Impairment mitigation and performance restoration, in *COST 255 Final Report*, *SP-1252*, chap. 5.3, Eur. Space Agency Publ. Div., Paris, March 2002b.

Crane, R. K., A two-component rain model for the prediction of attenuation statistics, *Radio Sci.*, *17*(6), 1371–1387, 1982.

Crane, R. K., *Electromagnetic Wave Propagation Through Rain*, *Wiley Ser. Remote Sens.*, 273 pp., John Wiley, New York, 1996.

Crane, R. K., and H. C. Shieh, A two-component rain model for the prediction of site diversity performance, *Radio Sci.*, *24*(6), 641–665, 1989.

Dennis, A. S., and F. G. Fernald, Frequency distributions of shower sizes, *J. Appl. Meteorol.*, *2*, 767–769, 1963.

Drufuca, G., Radar-derived statistics on the structure of precipitation patterns, *J. Appl. Meteorol.*, *16*, 1029–1035, 1977.

Féral, L., F. Mesnard, H. Sauvageot, L. Castanet, and J. Lemorton, Rain cell shape and orientation distribution in South-West of France, *Phys. Chem. Earth B*, *25*(10–12), 1073–1078, 2000.

Féral, L., H. Sauvageot, L. Castanet, and J. Lemorton, HYCELL—A new hybrid model of the rain horizontal distribution for propagation studies: 2. Statistical modeling of the rain rate field, *Radio Sci.*, *38*, doi:10.1029/2002RS002803, in press, 2003.

Goldhirsh, J., Two-dimensional visualization of rain cell structures, *Radio Sci.*, *35*(3), 713–729, 2000.

Goldhirsh, J., and B. Musiani, Rain cell size statistics derived from radar observations at Wallops Island, Virginia, *IEEE Trans. Geosci. Remote Sens.*, *24*(6), 947–954, 1986.

Konrad, T. G., Statistical models of summer rainshowers derived from fine-scale radar observations, *J. Appl. Meteorol.*, *17*, 171–188, 1978.

Lane, S. O., and W. L. Stutzman, Spatial rain rate distribution modeling for earth-space link propagation calculations, paper presented at Antennas and Propagation International Symposium, Union Radio Sci. Int., Quebec, Canada, 1980.

Lemorton, J., L. Castanet, V. Huot, and T. Marsault, A new opportunity for EHF propagation experiments, the EXPRESS campaign with the satellite STENTOR, *Int. J. Satell. Commun.*, *19*(3), 347–362, 2001.

Mesnard, F., and H. Sauvageot, Structural characteristics of rain fields, *J. Geophys.*, *108*, doi:10.1029/2002JD002808, in press, 2003.

Miller, J. R., A. S. Dennis, J. H. Hirsch, and D. E. Cain, Statistics of shower echoes in western North Dakota, paper

presented at Radar Meteorology Conference, Am. Meteorol. Soc., Houston, Tex., 1975.

Misme, P., and P. Waldteufel, A model for attenuation by precipitation on a microwave earth-space link, *Radio Sci.*, *15*(3), 655–665, 1980.

Nzeukou, A., and H. Sauvageot, Distribution of rainfall parameters near the coast of France and Senegal, *J. Appl. Meteorol.*, *41*(1), 69–82, 2002.

Paraboni, A., G. Masini, and C. Riva, The spatial structure of rain and its impact on the design of advanced TLC systems, paper presented at 4th Ka Band Utilization Conference, Venice, Italy, 1998.

Paraboni, A., F. Barbaliscia, C. Capsoni, and C. Riva, Small and large scale spatial distribution of precipitation, paper presented at GA, Union Radio Sci. Int., Maastricht, Netherlands, 2002.

Pawlina, A., and M. Binaghi, Radar rain intensity fields at ground level: New parameters for propagation impairments prediction in temperate regions, paper presented at 7th Commission F, Triennal Symposium, Union Radio Sci. Int., Ahmedabad, India, 1995.

Rogers, R. R., Radar-derived statistics on slant path attenuation at 10 GHz, *Radio Sci.*, *7*(6), 631–643, 1972.

Sauvageot, H., The probability density function of rain rate and the estimation of rainfall by area integrals, *J. Appl. Meteorol.*, *33*(11), 1255–1262, 1994.

Sauvageot, H., F. Mesnard, and R. S. Tenorio, The relation between the area-average rain rate and the rain cell size distribution parameters, *J. Atmos. Sci.*, *56*, 57–70, 1999.

Tenorio, R. S., H. Sauvageot, and S. Ramos-Buarque, Statistical studies of rain cell size distribution using radar data during squall line episodes in West Africa, paper presented at Third International Symposium on Hydrological Applications of Weather Radar, Sao Paulo, Brazil, 1995.

L. Castanet, L. Féral, and J. Lemorton, Département Electromagnétisme et Radar, ONERA, BP 4025, 2 avenue Edouard Belin, 31055 Toulouse, Cedex 4, France. (laurent.feral@onera.fr)

H. Sauvageot, Observatoire Midi-Pyrénées, Laboratoire d'Aérologie, Université Paul Sabatier, 31400 Toulouse, France.